Computers and Geotechnics 43 (2012) 111–123

Contents lists available at SciVerse ScienceDirect

Computers and Geotechnics

journal homepage: www.elsevier.com/locate/compgeo

Interpretation of unsaturated soil behaviour in the stress–saturation space II: Constitutive relationships and validations

An-Nan Zhou [a,*], Daichao Sheng [b,1], Scott W. Sloan [b,2], Antonio Gens [c,3]

[a] School of Civil, Environmental and Chemical Engineering, Royal Melbourne Institute of Technology (RMIT), Melbourne, VIC 3001, Australia
[b] Centre for Geotechnical and Materials Modelling(CGMM), School of Engineering, The University of Newcastle, Callaghan, NSW 2308, Australia
[c] Department of Geotechnical Engineering and Geosciences, Universitat Politecnica de Catalunya, Barcelona, Spain

ARTICLE INFO

Article history:
Received 23 May 2011
Received in revised form 20 February 2012
Accepted 21 February 2012
Available online 29 March 2012

Keywords:
Unsaturated soil
Constitutive modelling
Triaxial stress state
Effective degree of saturation
Bishop effective stress
Hydro-mechanical interaction
Experimental validation

ABSTRACT

Based on the equations for volume change and saturation variation proposed in the companion paper [37], an alternative constitutive framework is presented for interpreting coupled hydro-mechanical behaviour for unsaturated soils. In this new framework, all constitutive laws are built in the space of stress vs. degree of saturation. Suction is not involved explicitly in the constitutive model for unsaturated soils. The loading-collapse yield surface is derived based on the proposed volume change equation in the plane of the effective degree of saturation and the Bishop effective stress. The proposed volume change equation and the corresponding yield surface are generalised to three-dimensional stress states by incorporating with the Modified Cam-clay model, following the same procedure introduced in the Sheng–Fredlund–Gens (SFG) model. The basic properties and performance of the proposed constitutive model are then illustrated through numerical examples with various drying/wetting/loading paths. Finally, the proposed model is validated against a variety of experimental data including drained and undrained tests, isotropic and triaxial tests and reconstituted and compacted soils.

1. Introduction

A new volume change equation has been proposed in the preceding companion paper [37]. In the volume change equation, the soil compression index, which is assumed to be a function of the effective degree of saturation, is interpolated from the known compressibility at the fully saturated state and that at a dry state. A novel approach to simulate saturation variation (both hydraulic hysteresis and hydro-mechanical interaction) was then introduced, which enables the calculation of the effective degree of saturation under complex stress and suction paths. The proposed volume change equation in terms of Bishop's effective stress and degree of saturation gives a better explanation to the non-linear change of soil compressibility under constant suction.

The objective of the present paper is to demonstrate and validate a specific constitutive model constructed on the fundamental equations for volume change and saturation variation proposed in the companion paper [37].

The paper is organised as follows. Based on basic equations for volume change and saturation variation, the yield surface and constitutive relationships are developed following the general procedure presented in the SFG model [17], with the degree of saturation as a state variable or an additional variable in the stress space. The basic properties and performance of the proposed model are then illustrated through three numerical examples with different paths: i.e. (1) drying → isotropic loading → wetting-collapse, (2) drying → loading to full saturation → suction reduction, and (3) drying–wetting circle with different net stresses. Finally, the proposed model is validated against a variety of experimental data. The experimental validation involves both reconstituted unsaturated soils and compacted soils. The experimental results for model validation include: (1) suction-controlled isotropic loading and soaking tests, (2) undrained isotropic compression tests, (3) suction-controlled triaxial tests, and (4) undrained triaxial tests. A comparison between the predictions and the experimental data shows that the model broadly captures the essential behaviour of the tested soil in various conditions (drained/undrained, isotropic/triaxial, drying/wetting), which indicates that the fundamental equations proposed in Zhou et al. [37] and the specific model presented in this paper are a sound foundation for the description of hydromechanical behaviour of unsaturated soils.

* Corresponding author. Tel.: +61 3 99250407; fax: +61 3 96390138.
E-mail addresses: Annan.Zhou@rmit.edu.au (A.-N. Zhou), Daichao.Sheng@newcastle.edu.au (D. Sheng), Scott.Sloan@newcastle.edu.au (S.W. Sloan), Antonio.Gens@upc.edu (A. Gens).
[1] Tel.: +61 2 49215746; fax: +61 2 49216991.
[2] Tel.: +61 2 49216059; fax: +61 2 49216991.
[3] Tel.: +34 93 4016867; fax: +34 93 4017251.

0266-352X/$ - see front matter © 2012 Elsevier Ltd. All rights reserved.
http://dx.doi.org/10.1016/j.compgeo.2012.02.009

2. Constitutive relationships in the stress–saturation space

Following the original and Modified Cam-clay models [14,13,15], plastic volumetric strain (ε_v^p) is adopted as the hardening parameter here to develop the constitutive law from the volume change equation proposed previously. The yield surface can be derived from the contours of the constant plastic volumetric strain. In the plane of effective degree of saturation and effective mean stress, the intersection point between the yield surface and the p'-axis (where the effective degree of saturation is equal to one) is defined as the yield stress, p'_c.

2.1. Yield stress for isotropic conditions

The plastic volumetric strain of an arbitrary point on the normal consolidation line can be calculated through volume change equation, i.e. Eqs. (3) and (6) in Zhou et al. [37]:

$$\varepsilon_v^p = \frac{\lambda(S_e) - \kappa}{N} \ln p' \tag{1}$$

Meanwhile, the plastic volumetric strain can also be defined by the yield stress (p'_c) based on Terzaghi's effective stress principle for the fully saturated state:

$$\varepsilon_v^p = \frac{\lambda_0 - \kappa}{N} \ln p'_c \tag{2}$$

Combining Eqs. (1) and (2), we obtain the yield surface (i.e. the contour of constant plastic volumetric strain) for the yield stress p'_c:

$$p' = (p'_c)^{\beta}, \quad \beta = \frac{\lambda_0 - \kappa}{\lambda(S_e) - \kappa} \tag{3}$$

Because of the hydraulic hysteresis and hydro-mechanical interaction, the yield surface is not easy to illustrate in the plane of suction and mean net stress, such as in the traditional loading-collapse yield surface of the BBM [1]. But, as shown in Fig. 1, the yield surface can be plotted in the space of effective degree of saturation vs. effective stress (i.e. S_e—p' space). Fig. 1a shows the yield surfaces (at $p'_c = 10$ kPa) for different values of the fitting parameter a_1, Fig. 1b shows the yield surfaces ($a_1 = 1.0$) for various values of the yield stress (p'_c), and Fig. 1c shows the yield surfaces ($a_1 = 1.0$, and $p'_c = 10$ kPa) for various values of λ_d. The material parameters (such as λ_0, λ_d, and κ) are listed in Table 1.

2.2. Generalising constitutive relationships to triaxial conditions

The Modified Cam-clay model (MCC, [13]) is employed as the starting point for extending the constitutive model from an isotropic state to a triaxial stress state. If we need to model the complicated stress–strain behaviour of real soils (such as softening behaviour, peak strength, shear-dilation, kinematic hardening and time-dependency), the MCC model can be replaced by a number of advanced saturated models, such as a bounding surface model, a sub-loading surface model, a three-dimensional stress model, a density-dependent model, or an elastic–viscoplastic model [3,6,8,34,33,35]. Some attempts to apply these advanced models into unsaturated constitutive modelling can be found in the recent literature (e.g. [22,4,32,10,30,9,12]). Similarly, the proposed isotropic constitutive model can also be combined with these advanced saturated models if necessary.

The MCC yield surface (ellipse) for a triaxial stress state can be expressed as

$$q^2 - M^2 p'(p'_x - p') \equiv 0 \tag{4}$$

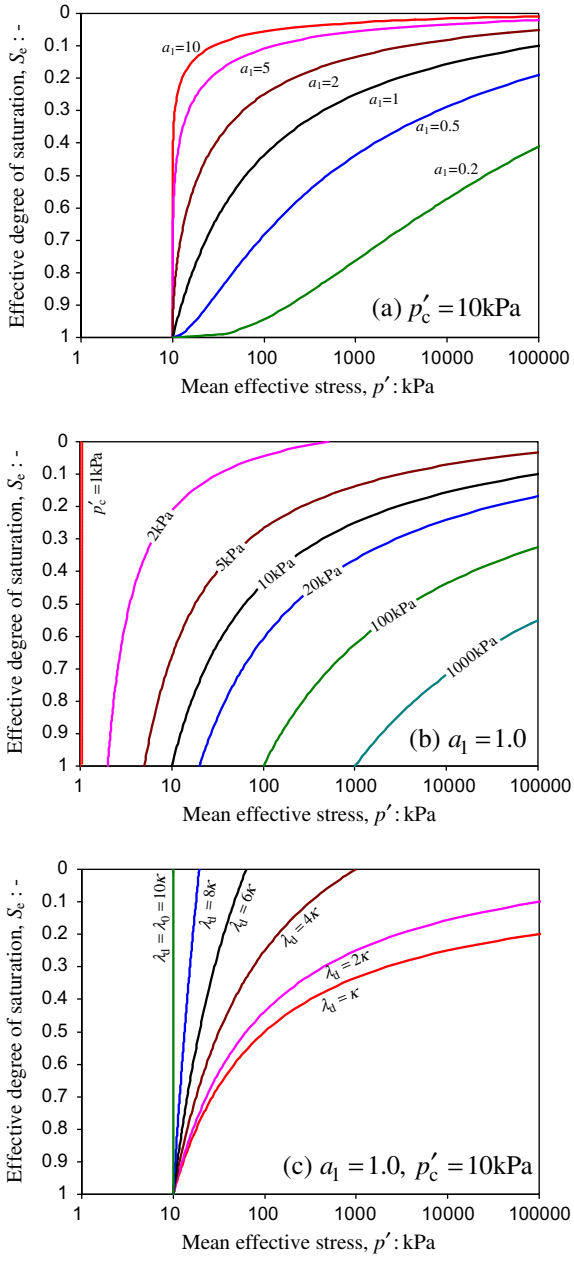

Fig. 1. Yield surfaces in the plane of effective degree of saturation vs. mean effective stress: (a) variation of yield surfaces with a_1, (b) variation of yield surfaces with yield stress, (c) variation of yield surfaces with λ_d.

Table 1
Parameters for numerical study on proposed model.

Parameters: Mechanical component	Parameters: Hydraulic component
Elastoplastic compressibility $\lambda_0 = 0.2$, $\lambda_d = 0.04$	SWCC (main drying and wetting) $a_d = 200$ kPa, $n_d = 0.5$, $m_d = 2.5$ $a_w = 50$ kPa, $n_w = 0.5$, $m_w = 2.5$ Residual degree of saturation $S_r^{res} = 0$
Elastic compressibility $\kappa = 0.02$	SWCC (scanning) $b = 3.0$
Influence of S_e on compressibility $a_1 = 1.0$	Influence of deformation on S_e $a_2 = 0.5$ for Case 1 $a_2 = 0.05$ for Case 2

where q is the deviator stress; M is the stress ratio (q/p') at the critical state which is assumed to be independent of the saturation status and suction levels [28,11,36], but can vary with the Lode's angle [18], and p'_x is the intersection point between the MCC ellipse and the p'-axis. For both saturated and unsaturated soils, the yield surface in p'–q space can be written using Eqs. (3) and (4). Combining these equations we obtain

$$p'_x = \frac{q^2}{M^2 p'} + p' = (p'_c)^{\beta} \Longleftrightarrow \left(\frac{q^2}{M^2 p'} + p'\right)^{\frac{1}{\beta}} = p'_c \tag{5}$$

The plastic volumetric strain (ε_v^p) is adopted as the hardening parameter and the hardening law is defined as follows:

$$\frac{dp'_c}{p'_c} = \frac{1+e}{\lambda_0 - \kappa} d\varepsilon_v^p \tag{6}$$

The yield surfaces for triaxial stress states are illustrated in the plane of p'–S_e–q in Fig. 2. An associated flow rule for MCC is also accepted here for simplicity, i.e.:

$$\frac{d\varepsilon_v^p}{d\varepsilon_d^p} = \frac{M^2 p'^2 - q^2}{2p'q} \tag{7}$$

where $d\varepsilon_v^p$ is the incremental plastic volumetric strain and $d\varepsilon_d^p$ is the incremental plastic deviator strain.

3. Numerical study

In this section, some numerical examples are used to illustrate the performance of the proposed hydro-mechanical model. Some typical mechanical (isotropic) or hydraulic loading/unloading paths are employed, such as (1) drying–loading–wetting (to the saturated state), (2) drying–loading (to fully saturated state)-suction reduction, (3) and a drying–wetting cycle under different stresses. The parameters for a hypothetical soil used in the numerical study are listed in Table 1. The residual degree of saturation is assumed to zero, i.e. $S_r^{res} = 0$, and $S_r = S_e$.

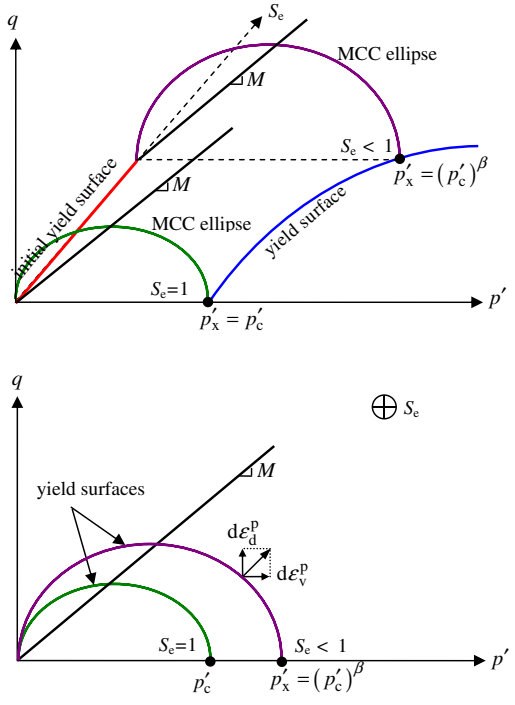

Fig. 2. Yield surfaces under triaxial stress state.

3.1. Case 1: Drying → isotropic loading → wetting-collapse

The performance of the proposed model under a drying–loading–wetting circle is investigated in the first example. The net stress-suction path is illustrated in Fig. 3a. In the first phase, the slurry soil, (point A, fully saturated, initial mean net stress $\bar{p} = 1$ kPa, initial suction $s = 0$ kPa, initial yield stress $p'_c = 1$ kPa) is dried under a constant net stress to point B (unsaturated, mean net stress $\bar{p} = 1$ kPa, suction $s = 200$ kPa). The specimen is then loaded from point B to point C (unsaturated, mean net stress $\bar{p} = 1000$ kPa, suction $s = 200$ kPa) under a constant suction. After that, holding the net stress constant, the soil is wetted from point C to point D (fully saturated, mean net stress $\bar{p} = 1000$ kPa, suction $s = 0$ kPa). Fig. 3b and c shows the mechanical responses over this net stress-suction path. The relationship between the voids ratio and the mean net stress $(v - \ln \bar{p})$ is plotted in Fig. 3b, and that between the voids ratio and the suction $(v - \ln s)$ in Fig. 3c. Some basic behaviour features of unsaturated soils, such as the apparent consolidation due to drying as well as wetting-collapse, can therefore be simulated by the proposed model.

The relationship between the degree of saturation and the mean net stress $(S_r - \ln \bar{p})$ is drawn in Fig. 3d and that between the degree of saturation and the suction $(S_r - \ln s)$ in Fig. 3e. The increase of the degree of saturation due to loading and the non-linear scanning wetting curve is modelled by the proposed constitutive relationships. It is important to note that the scanning curve can lie outside the primary branch as predicted in Fig. 3e if a change of net stress is involved. In Fig. 3b and d, the yielding point (point Y) due to loading is indicated by symbol '★'. Fig. 3f shows the effective stress path in the plane of the effective degree of saturation vs. the effective mean stress $(S_e - \ln p')$. This figure illustrates the evolution of the yield surface as well as the elastoplastic/elastic responses of this hypothetical soil.

The drying process for the normally consolidated saturated soil generates an elastoplastic compression and expands the yield surface while changing its shape. At turning point E that is indicated by symbol '☆', the stress point moves to the inside of the yield surface (the yield surface keeps unchanged) and a purely elastic response occurs after that. Beyond point E, the shrinkage volume due to drying sharply decreases (only elastic compression occurs), which is in accordance with the experimental results presented by Cunningham et al. [5] (see test data presented in Fig. 7). Loading after drying leads to the movement of the stress point towards the yield surface. At yielding point Y which is indicated by symbol '★', the stress point touches the yield surface and generates an elastoplastic response. The wetting path CD first causes an elastoplastic volume decrease (collapse) and then a small elastic volume increase, Fig. 3c. The point D′ corresponds to the full saturation, as shown in Fig. 3e, which also explains the plateau observed along the path D′D in Fig. 3c. Point D is slightly within the yield surface of point D′ in Fig. 3f. The elastic/elastoplastic transition shown in Fig. 3f is consistent with the volume and saturation changes shown in Fig. 3b–e.

3.2 Case 2: Drying → loading to full saturation → suction reduction

In this numerical example, the performance of the proposed model is studied over a wide range of mean net stress values. The net stress-suction path is shown in Fig. 4a. Prior to compression, the unsaturated specimen (point B: unsaturated, mean net stress $\bar{p} = 1$ kPa, suction $s = 200$ kPa) is dried from a slurry state (point A: fully saturated, initial mean net stress $\bar{p} = 1$ kPa, initial suction $s = 0$ kPa, and initial yield stress $p'_c = 1$ kPa). The specimen is then loaded from point B to point C (fully saturated, mean net stress $\bar{p} = 20$ MPa, suction $s = 200$ kPa) under the constant suction of 200 kPa. After that, the suction is reduced to point D under

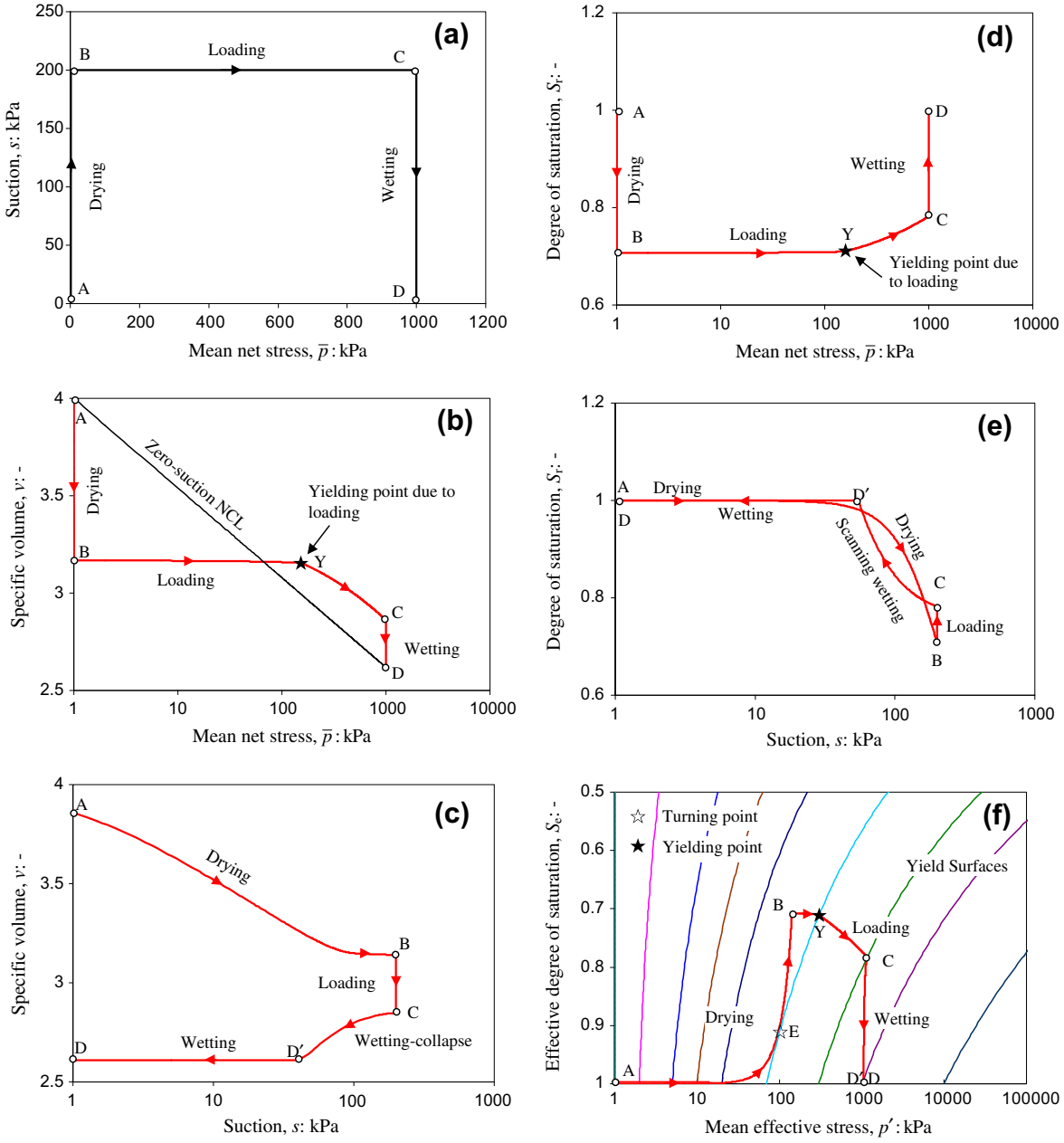

Fig. 3. Drying–loading (isotropic)–wetting path and the calculated responses: (a) s vs. $\bar{p}$, (b) v vs. $\bar{p}$, (c) v vs. s, (d) S_r vs. $\bar{p}$, (e) S_r vs. s, (f) S_e vs. p'.

constant net stress (fully saturated, mean net stress $\bar{p} = 20$ MPa, suction $s = 0$ kPa). The relationship between the voids ratio and the mean net stress ($v - \ln \bar{p}$) is plotted in Fig. 4b. Along the loading path BC, the soil yields at point Y. The curve between points Y and C therefore corresponds to the so-called constant-suction normal compression of the soil and is clearly not a straight line. It approaches the normal compression line for the saturated soils smoothly, indicating it is indeed possible to compress the soil to full saturation under constant suction. Fig. 4c shows the volume change against the logarithmic suction. Since the soil at point C is already fully saturated, the wetting path CD only causes a small elastic volume expansion.

The corresponding change of the degree of saturation is plotted against the mean net stress in Fig. 4d and against the suction in Fig. 4e. Path AB and path CD are both on the primary (main) drying and wetting curves, respectively, but for different net stresses. Fig. 4f shows the compression curve in the plane of the specific volume vs. the effective mean stress ($v - \ln p'$). As shown in Fig. 4f, the slope of the compression curve keeps increasing during loading and the state point eventually moves back to the saturated NCL. Fig. 4g shows the effective stress path, as well as the evolution of the yield surface in the plane of the effective degree of saturation vs. the effective mean stress ($S_e - \ln p'$). It shows that the second part of the drying path AB causes only elastic volume change and the turning point (E) is marked by symbol '☆'. The first part of the loading path BC is also elastic and the yield point (Y) is indicated by symbol '★'. Finally, Fig. 4h shows the potential wetting-induced collapse volume vs. the mean net stress, which mimics the experimental results shown in Fig. 4 in Zhou et al. [37]. The point where the fully saturated NCL is reached by loading is indicated by symbol '△' in Fig. 4b–h.

3.3. Case 3: Drying–wetting circle under different net stresses

In the last numerical example, we examine the performance of the proposed model for drying–wetting cycles ($S_r - \ln s$) under dif-

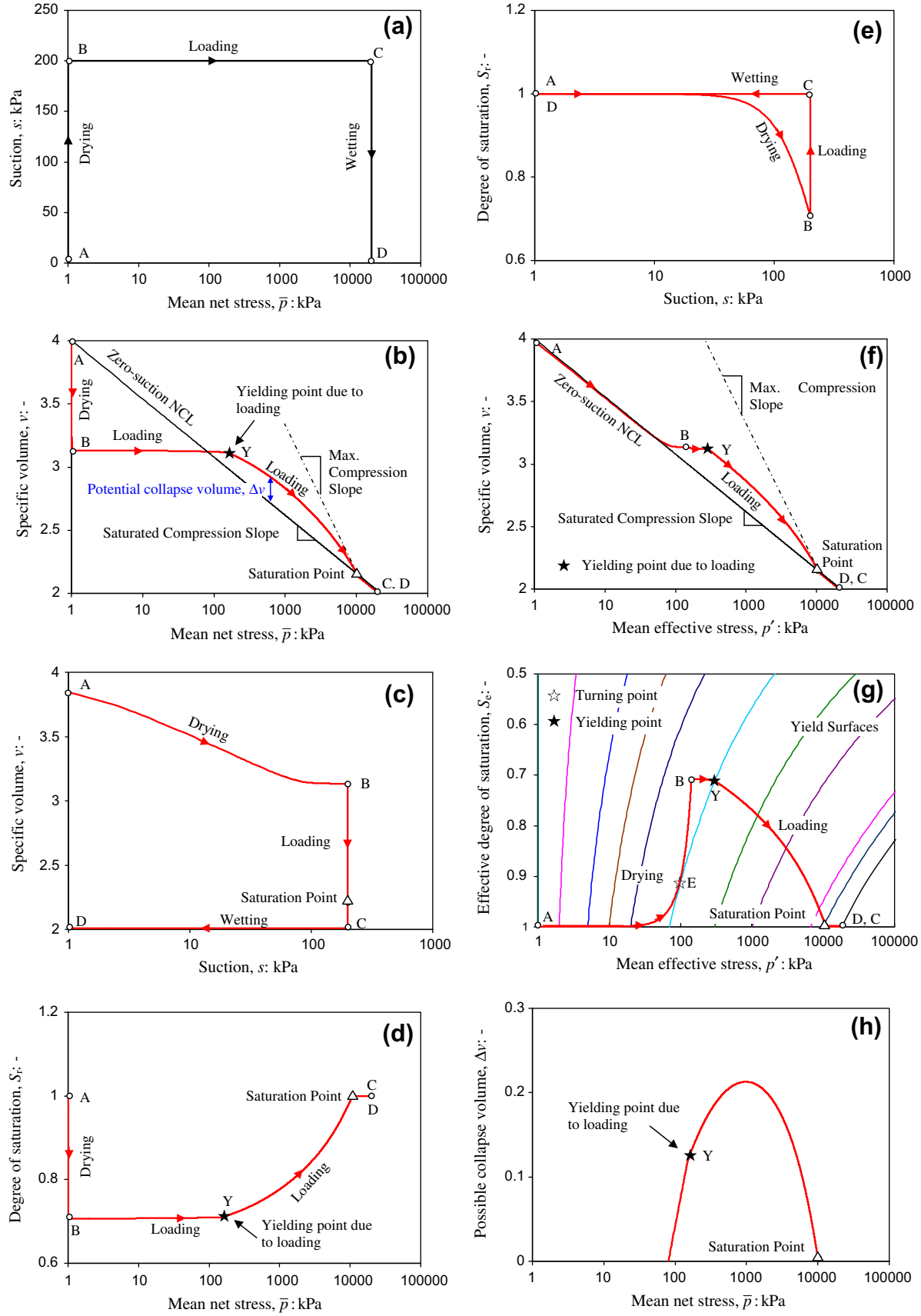

Fig. 4. Drying–loading (isotropic, to fully saturated) path and calculated responses: (a) s vs. $\bar{p}$, (b) v vs. $\bar{p}$, (c) v vs. s, (d) S_r vs. $\bar{p}$, (e) S_r vs. s, (f) v vs. p', (g) S_e vs. p', (h) Δv vs. $\bar{p}$.

ferent mean net stresses (1 kPa, 200 kPa and 1000 kPa), as shown in Fig. 5. The drying–wetting cycle ($S_r - \ln s$) under 1 kPa of load is adopted as the reference cycle to exhibit the effect of the mean net stress on the hydraulic response. All the hydraulic parameters

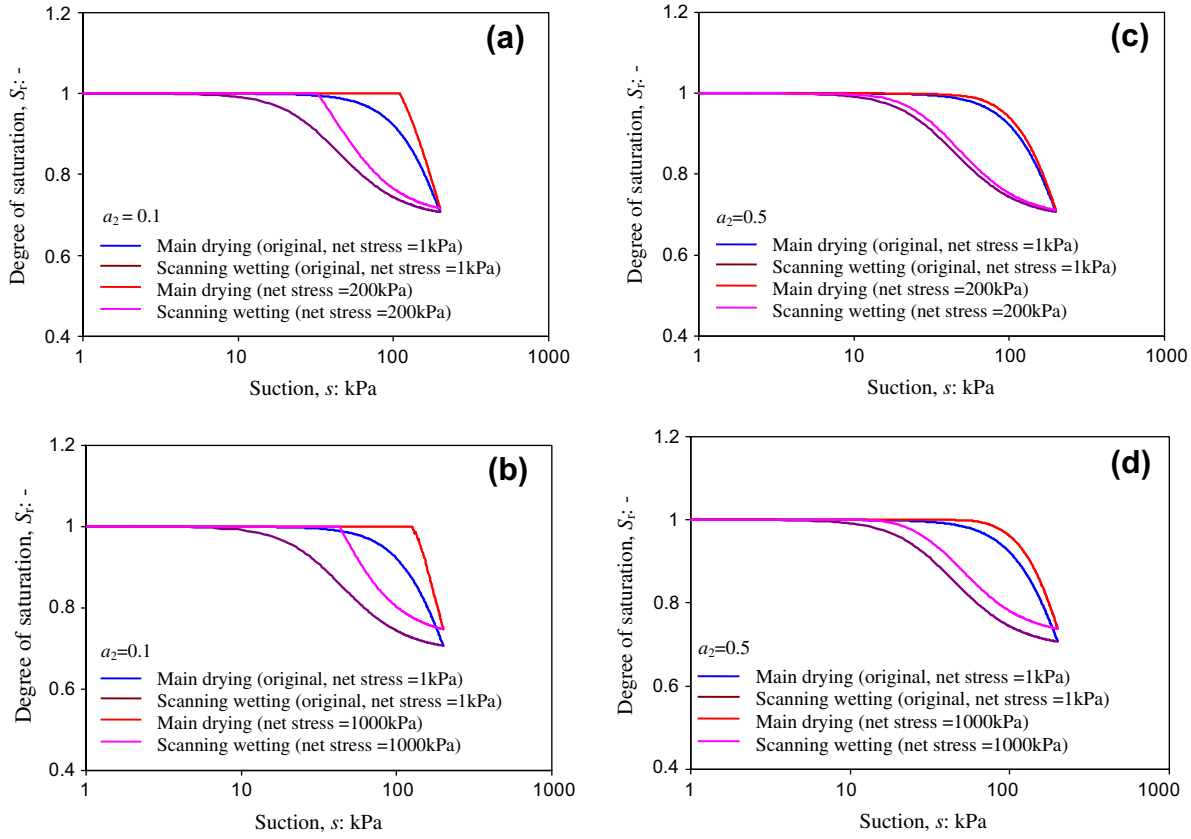

Fig. 5. Drying–wetting circles under different mean net stresses and calculated responses: (a) $a_2 = 0.1$, $\bar{p} = 200$ kPa, (b) $a_2 = 0.1$, $\bar{p} = 1000$ kPa, (c) $a_2 = 0.5$, $\bar{p} = 200$ kPa, (d) $a_2 = 0.5$, $\bar{p} = 1000$ kPa.

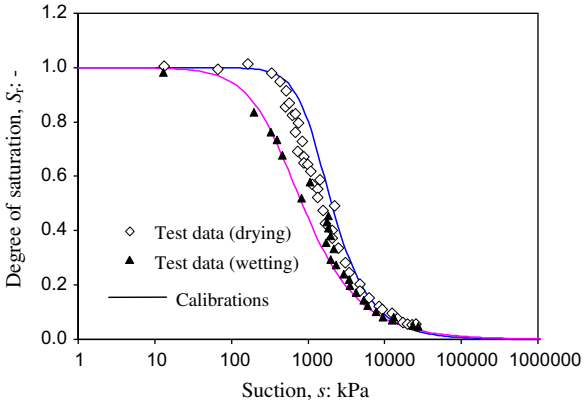

Fig. 6. Soil–water characteristic curves (main drying and main wetting branches) of silty clay and calibrations (data after [5]).

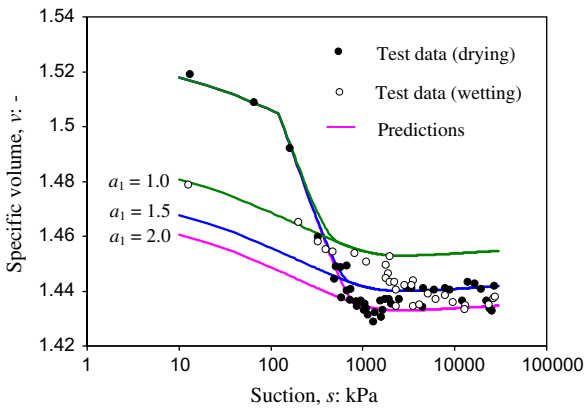

Fig. 7. Drying and wetting test results and model simulations (data after data after [5]).

Table 2
Parameters for reconstituted silty clay.

Parameters: Mechanical component	Parameters: Hydraulic component
Elastoplastic compressibility $\lambda_0 = 0.043$	SWCC (main drying) $a_d = 1200$ kPa, $n_d = 0.45$, $m_d = 2.5$
Elastic compressibility $\kappa = 0.007$	SWCC (main wetting) $a_w = 450$ kPa, $n_w = 0.55$, $m_w = 1.5$
	Residual degree of saturation $S_r^{res} = 0$
Critical state $M = 1.25$ ($\varphi' = 31°$)	SWCC (scanning) $b = 3.0$
Influence of S_e on compressibility $a_1 = 2.0$	Influence of deformation on S_e $a_2 = 1.0$

listed in Table 1 correspond to the reference cycle. Fig. 5a and b shows the calculated drying–wetting curves ($S_r - \ln s$) under net stresses of 200 kPa and 1000 kPa, respectively, with the fitting parameter (a_2) equal to 0.1. Fig. 5c and d shows similar plots but for a fitting parameter of $a_2 = 0.5$. All simulations indicate that the increase of net stress leads to the shifting (upwards) of the drying–wetting curve, which is supported by the experimental data in literature (e.g. [16,7,27]). Besides, Fig. 5 also indicates that the fitting parameter (a_2 controls the shifting patterns of the drying–wetting curves ($S_r - \ln s$) due to the net stress change. Comparison between Fig. 5a and c as well as that between Fig. 5b and d reveals that the higher value of parameter a_2 leads to a more distinct upward shifting of SWCC for the same increase in mean net stress.

4. Experimental validations

Experimental results from (1) suction-controlled isotropic loading and soaking tests, (2) undrained isotropic compression tests, (3) suction-controlled triaxial tests, as well as (4) undrained triaxial tests are presented to validate the proposed constitutive model. Both reconstituted soil and compacted soil are considered in the experimental validations.

4.1. Experimental behaviour of reconstituted unsaturated soil and model simulations

Cunningham et al. [5] presented the results of a series of isotropic compression tests on reconstituted silty clay that comprised a mix of 20% pure Speswhite kaolin, 10% London clay and 70% silica silt. The slurry soil was isotropically preconsolidated to 130 kPa, i.e. the initial yield stress is 130 kPa. The main drying and main wetting branches of the soil–water characteristic curve, as well as the fitting equations [31], are plotted in Fig. 6. The calibration parameters for the main drying branch are $a_d = 1200$ kPa, $n_d = 0.45$, and $m_d = 2.5$, while those for the main wetting branch are $a_w = 450$ kPa, $n_w = 0.55$, and $m_w = 1.5$. The parameter for the scanning law (b) is assumed to be 3, and the residual degree of saturation is set to zero, i.e. $S_r^{res} = 0$. The parameters for the fully saturated counterpart are $\lambda_0 = 0.043$, $\kappa = 0.007$, and $M = 1.25$ as reported in Cunningham et al. [5]. As no test data is available for a fully dried sample, we assume the compressibility of the dried soil is equal to the elastic compressibility so that $\lambda_d = \kappa = 0.007$. In accordance with the approach described in Zhou et al. [37], the fitting parameter for the compressibility (a_1) is set to 2.0 and the fitting parameter for the SWCCs (a_2) is set to 1.0. All the parameters for this reconstituted soil listed in Table 2.

The experimental results of the drying–wetting test presented by Cunningham et al. [5], together with the model simulations, are shown in Fig. 7. For the initial drying, when the suction is less than the initial yield stress (130 kPa), the response is purely elastic. Once the suction level goes beyond the initial yield stress, the soil behaves elastoplastically. As shown in Fig. 7, the model simulation ($a_1 = 2$) reproduces the key features of the drying test very well but is less satisfactory for the wetting test. The classical MCC elastoplastic framework might be a reason for this. Adoption of the bounding surface concept, or other cyclic models that take into account the stress hysteresis (unloading/reloading hysteresis), may give a better prediction for wetting tests. Fig. 7 also shows the model simulations for different values of the parameter a_1. This indicates that the drying test is an alternative way to calibrate the fitting parameter (a_1), provided the main drying branch of the SWCC is known. To this end, Eq. (7) in Zhou et al. [37] can be expanded as

$$-\mathrm{d}v = [\lambda_0 - (1-S_e)^{a_1}(\lambda_0-\kappa)]\frac{s\mathrm{d}S_e + S_e\mathrm{d}s}{\bar{p}+S_e s} + a_1(1-S_e)^{a_1-1}(\lambda_0-\kappa)\ln(\bar{p}+S_e s)\mathrm{d}S_e \quad (8)$$

In a drying test, the relationship between the effective degree of saturation and the suction is defined by the main drying branch (i.e. Eqs. (10) and (11) in [37]). Therefore, Eq. (8) can be reformulated as

$$-\frac{\mathrm{d}v}{\mathrm{d}s} = \left[\lambda_0 - (1-S_{ed})^{a_1}(\lambda_0-\kappa)\right]\frac{s\frac{\partial S_{ed}}{\partial s} + S_{ed}}{\bar{p}+S_{ed}s} + a_1(1-S_{ed})^{a_1-1}(\lambda_0-\kappa)\ln(\bar{p}+S_{ed}s)\frac{\partial S_{ed}}{\partial s} \quad (9)$$

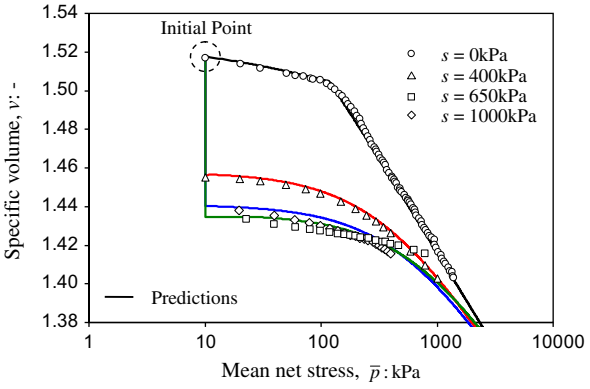

Fig. 8. Drying and compression test results and model simulations (data after [5]).

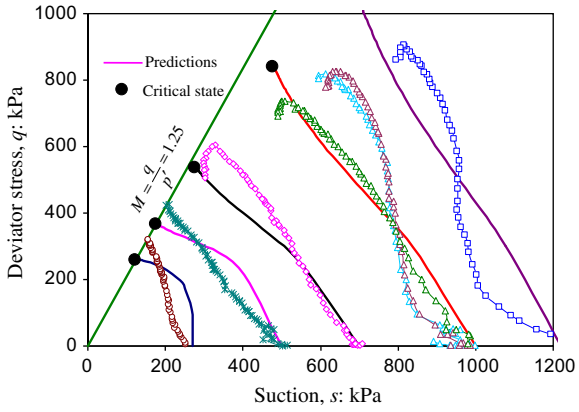

Fig. 9. Unconfined undrained tests with different initial suctions and model simulations (data after [5]).

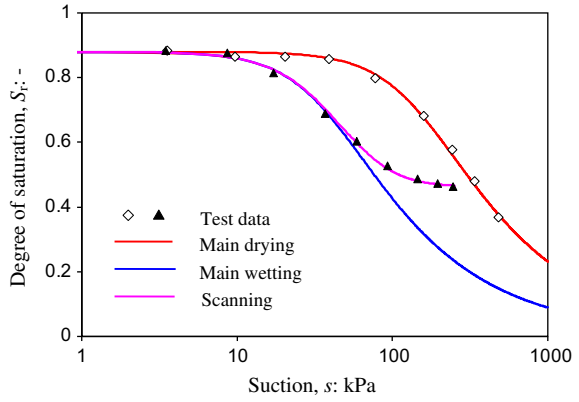

Fig. 10. Soil–water characteristic curves (main drying, main wetting branches and scanning curve) of Pearl clay and model simulations (data after [20]).

Table 3
Parameters for compacted Pearl clay.

Parameters: Mechanical component	Parameters: Hydraulic component
Elastoplastic compressibility $\lambda_0 = 0.13$	SWCC (main drying) $a_d = 150$ kPa, $n_d = 0.35$, m_d=2.0
Elastic compressibility $\kappa = 0.03$	SWCC (main wetting) $a_w = 38$ kPa, $n_w = 0.35$, $m_w = 2.0$
	Residual degree of saturation $S_r^{res} = 0$
Critical state $M = 1.12$	SWCC (scanning) $b = 4.0$
Influence of S_r on compressibility $a_1 = 1.7$	Influence of deformation on S_r $a_2 = 0.1$

where both S_{ed} and $\partial S_{ed}/\partial s$ are functions of the suction and are defined by Eqs. (10) and (11) in Zhou et al. [37].

Cunningham et al. [5] also conducted a series of suction-controlled isotropic compression tests under varying suctions (s = 0, 400 kPa, 650 kPa and 1000 kPa, respectively). The test data as well as the model simulations are shown in Fig. 8. The comparisons indicate that the predicted curves match the experimental data well. It is important to note that there is only one initial state (s = 0) used for all predictions. The initial states for other suction levels (s = 400 kPa, 650 kPa and 1000 kPa, respectively) are calculated through the drying process from the initial state at zero suction. This series of experimental validations also indicate that deformation due to an increase of suction and compression due to loading under constant suction can be described within a unified framework.

Finally, Cunningham et al. [5] undertook a series of unconfined shearing tests in which the samples were dried on the bench to a variety of predetermined moisture contents, corresponding to suctions in the range of 270–1220 kPa. The initial degree of saturation for each sample can be found through the main drying curve shown in Fig. 6, with initial suction level indicated in Fig. 9. The samples were then sheared under constant moisture content (undrained) conditions to failure. Throughout shearing, suction probes were used to monitor the suction changes within the specimens. Since all tests were undertaken in a simple loading frame without a confining medium, no volume change measurement was possible. Fig. 9 compares the test data with the model simulations, where it can be seen that the proposed model captures the key stress–strain features of the unsaturated reconstituted soil behaviour under undrained loading. The predicted shear strength is a little higher than the measured strength, which is probably due to the expression for the effective stress that is used (see Eq. (2) in [37]). Sheng et al. [19] compared several shear strength criteria and concluded that Eq. (2) in Zhou et al. [37] is not the best expression for predicting the shear strength of unsaturated soils. Better predictions can be obtained from the definition:

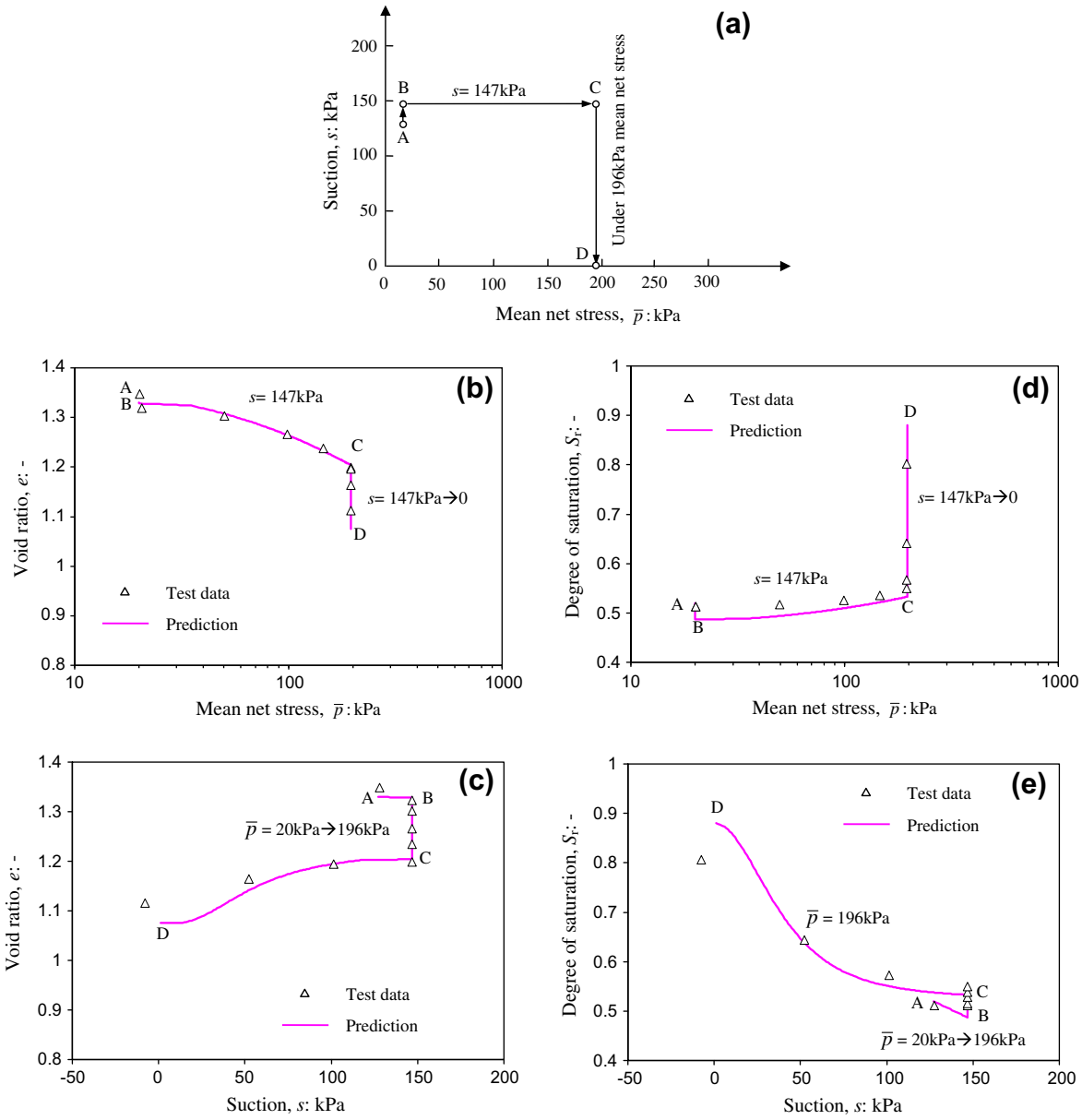

Fig. 11. Experimental results (data after [20]) of suction-controlled isotropic compression test (s = 147 kPa) and wetting test (s = 147 kPa → 0) on compacted Pearl clay, as well as model simulations: (a) stress path (s vs. $\bar{p}$), (b) e vs. $\bar{p}$, (c) e vs. s, (d) S_r vs. $\bar{p}$, and (e) S_r vs. s.

$$\sigma'_{ij} = \bar{\sigma}_{ij} + (S_e)^{a_3} s\delta_{ij} \quad (10)$$

where a_3 is a fitting parameter. If the above equation is adopted, the shear strength equation embedded in the proposed model will be identical with the shear strength criterion proposed by Toll and Ong [29]. The comparisons given in Sheng et al. [19] indicate that this shear strength criterion gives the best predictions of eight options that are available in the literature. Alonso et al. [2] also indicated Eq. (10) is an alternative way to express the Bishop effective stress. Adoption of this equation, which is a non-linear function of S_e, will possibly improve the model capacity, especially in predicting shear strength. However, such a non-linear function of S_e will add another fitting parameter (a_3) to the model.

4.2. Experimental behaviour of compacted unsaturated soil and model simulations

Sun et al. [21,20,23–26] conducted a series of experimental investigations on the mechanical and hydraulic properties of a compacted Pearl clay. Pearl clay contains 50% silt and 50% clay. Its liquid limit is 49% and its plasticity index is 22. The experimental soil–water characteristic curves (both main drying and main wetting branches, and scanning curve under zero net stress) as well as the fitting equations are plotted in Fig. 10. The parameters for the main drying curve are calibrated as a_d = 150 kPa, n_d = 0.35, and m_d = 2, while the parameters for the main wetting curve are estimated as a_d = 38 kPa, n_d = 0.35, and m_d = 2 based on the wetting scanning curve. The fitting parameter for the scanning curve (b) is equal to 4. The residual degree of saturation (S_r^{res}) is set to zero, and the degree of saturation at zero suction (S_r^0) is set to 0.88. The soil parameters for fully saturated Pearl clay are λ_0 = 0.13, κ = 0.03, and M = 1.12 as reported in Sun et al. [23], and the compressibility index of dried Pearl clay is assumed for simplicity to be equal to the elastic compressibility index, i.e. $\lambda_d = \kappa$ = 0.03. Following the approach demonstrated in Zhou et al. [37], the calibrated parameter (a_1) for the compressibility is 1.7 and the calibrated parameter (a_2) for the SWCCs is 0.1. The parameters used in all the simulations are listed in Table 3.

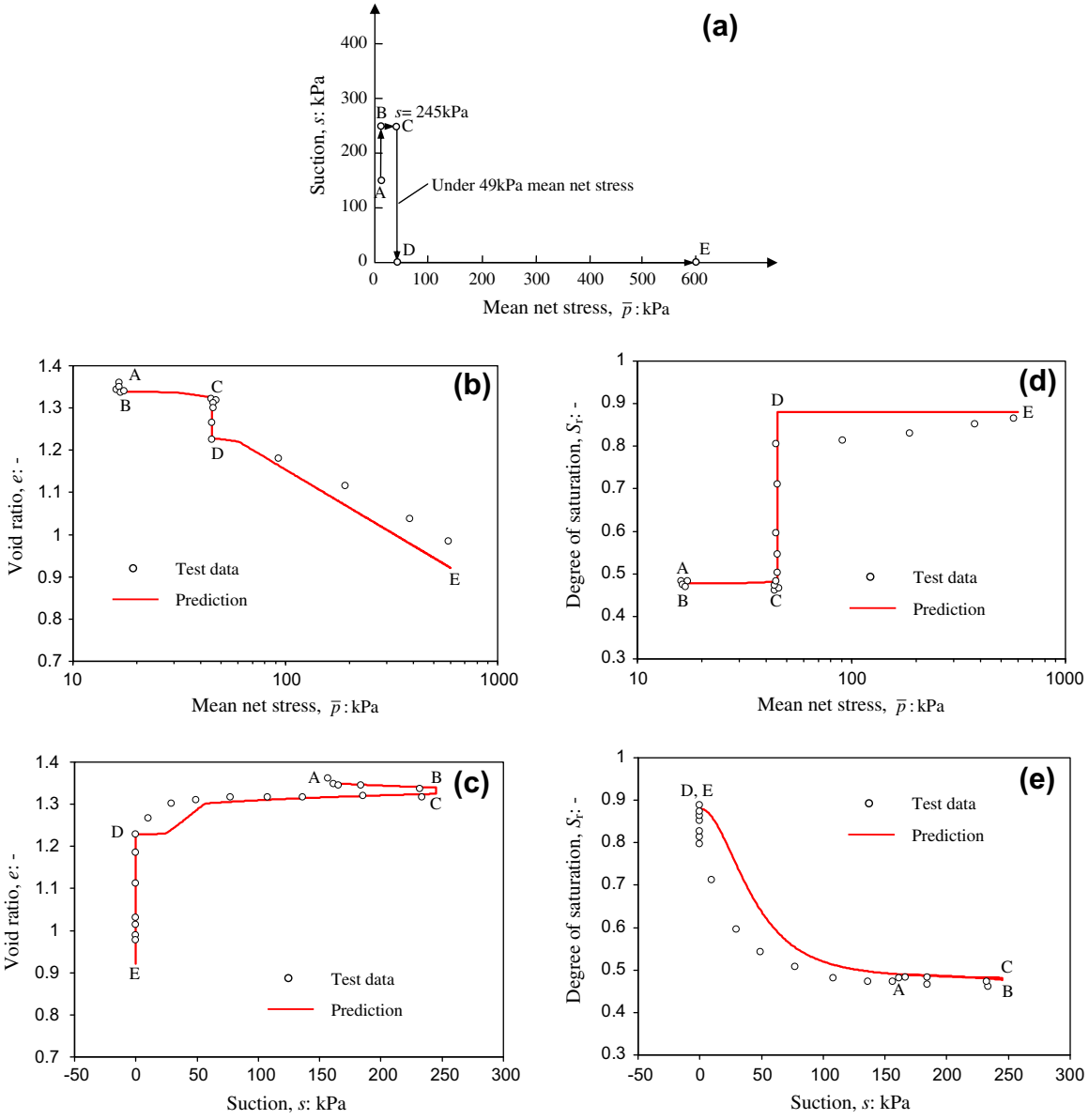

Fig. 12. Experimental results (data after [20]) of suction-controlled isotropic compression test (s = 245 kPa) and wetting test (s = 245 kPa → 0) on compacted Pearl clay, as well as model simulations: (a) stress path (s vs. $\bar{p}$), (b) e vs. $\bar{p}$, (c) e vs. s, (d) S_r vs. $\bar{p}$, (e) S_r vs. s.

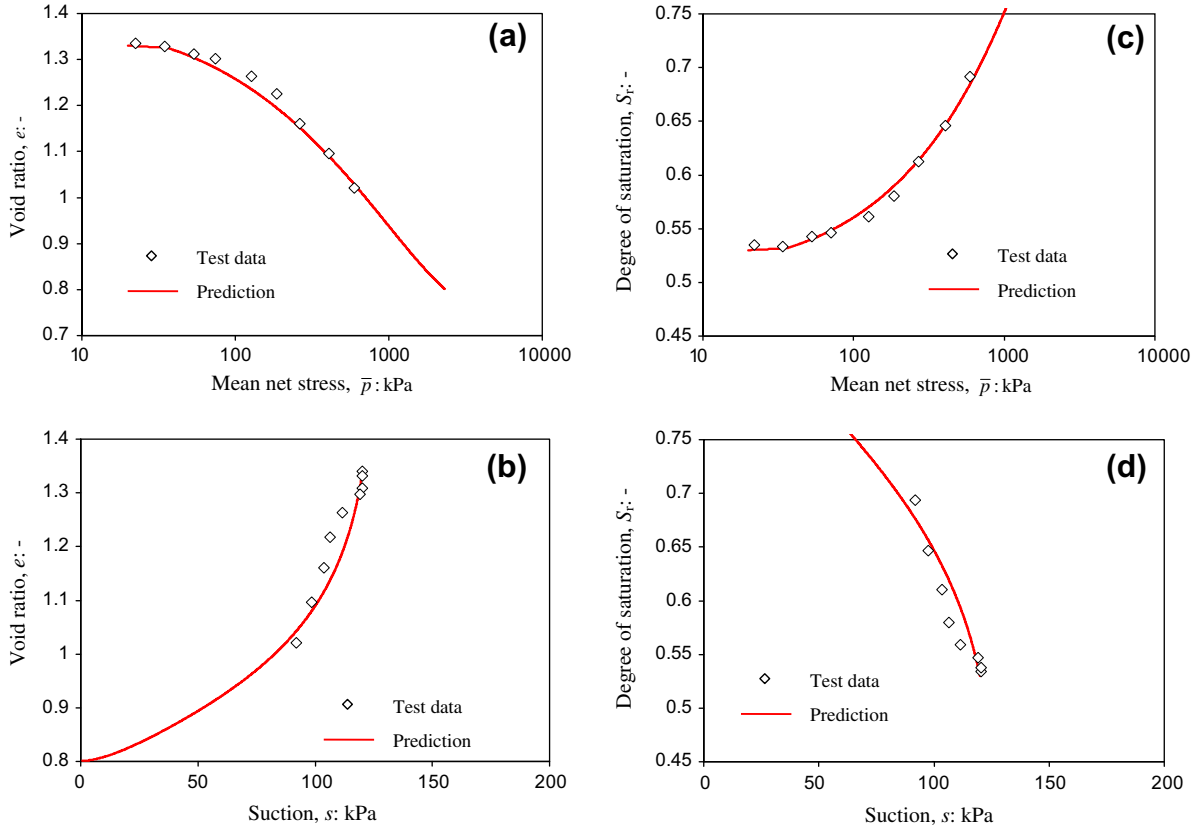

Fig. 13. Experimental results (data after [25]) of the undrained isotropic compression test on compacted Pearl clay as well as model simulations: (a) e vs. $\bar{p}$, (b) e vs. s, (c) S_r vs. $\bar{p}$, (d) S_r vs. s.

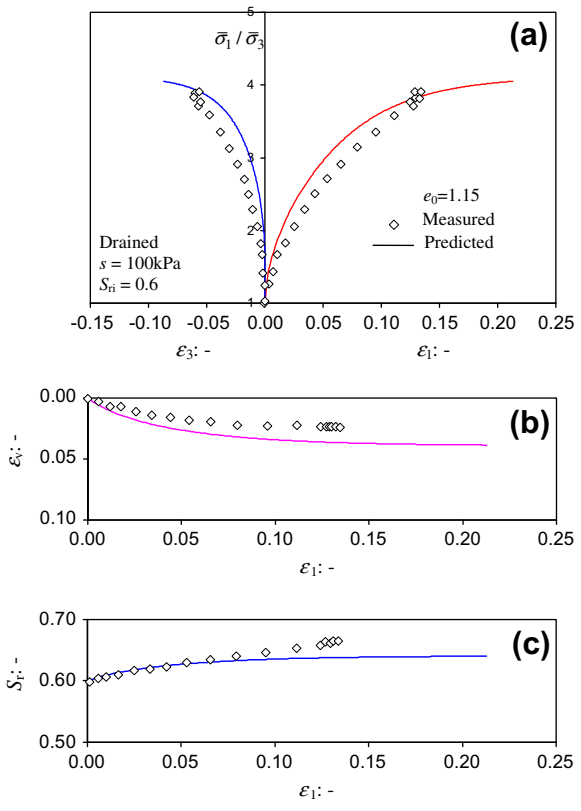

Fig. 14. Experimental results (data after [26]) of suction-controlled triaxial compression test on compacted Pearl clay (s = 100 kPa, S_{ri} = 0.6) as well as model simulations: (a) $\bar{\sigma}_1/\bar{\sigma}_3$ vs. ε_1 and ε_3, (b) ε_v vs. ε_1 and (c) S_r vs. ε_1.

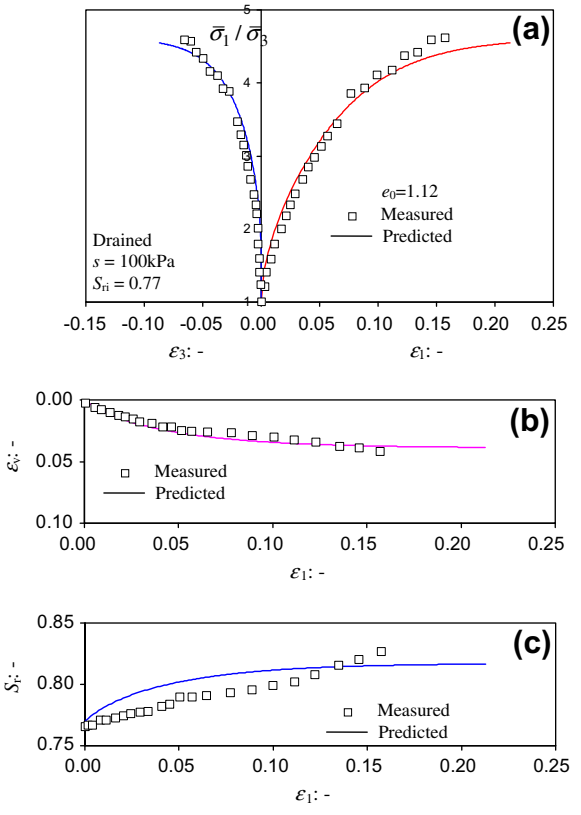

Fig. 15. Experimental results (data after [26]) of suction-controlled triaxial compression test on compacted Pearl clay (s = 100 kPa, S_{ri} = 0.77) as well as model simulations: (a) $\bar{\sigma}_1/\bar{\sigma}_3$ vs. ε_1 and ε_3, (b) ε_v vs. ε_1 and (c) S_r vs. ε_1.

Sun et al. [24] presented two suction-controlled isotropic compression (with soaking) tests. In the first series, the compacted soil sample with an initial suction of about 130 kPa is dried to the target suction of 147 kPa under a constant net stress of ~20 kPa (path A → B in Fig. 11a). After that, the sample is compressed to a mean net stress of 196 kPa under the constant suction of 147 kPa (path B → C in Fig. 11a), and finally soaked to zero suction (path C → D in Fig. 11a). In the second series, the compacted soil sample with an initial suction of about 150 kPa is first dried to the target suction of 245 kPa under a constant net stress of ~20 kPa (path A → B in Fig. 12a). Afterwards, the soil sample is loaded to a mean net stress of 49 kPa under the constant suction of 245 kPa (path B → C in Fig. 12a), and then soaked to zero suction under constant net stress (path C → D in Fig. 12a). The specimen is subsequently loaded to 598 kPa under zero suction (path D → E in Fig. 12a). The data from these two series of tests, as well as the model predictions, are plotted in Fig. 11 (suction = 147 kPa) and Fig. 12 (suction = 245 kPa), respectively. The volume changes are plotted against mean net stress in Figs. 11b and 12b, and against suction in Figs. 11c and 12c. These figures show that the predicted volume changes agree well with the experimental data, particularly in Fig. 11b and c. The changes of degree of saturation are plotted against mean net stress in Figs. 11d and 12d, and against suction in Figs. 11e and 12e. Again the predictions for the first series of the tests are remarkably good. The predictions for the second series of the tests are less accurate, though still quite reasonable. Overall, the proposed model seems to provide reasonable predictions of both the mechanical (e–$\bar{p}$ and e–s plots) and hydraulic behaviour (S_r–$\bar{p}$ and S_r–s plots) of the unsaturated compacted Pearl clay.

In addition to the suction-controlled isotropic compressions, Sun et al. [25] also investigated the hydro-mechanical properties of compacted Pearl clay under an undrained isotropic stress state. The initial suction is 22 kPa, and the initial mean net stress is 22.5 kPa. The initial degree of saturation is 0.53 and the initial void ratio is 1.34. The sample with the above initial states was isotropically compressed (the mean net stress increases to about 600 kPa) and the soil mechanical and hydraulic responses were monitored. Fig. 13 compares the predicted volume changes and saturation changes with the experimental results. The predicted volume and saturation changes against mean net stress agree very well with the experimental data (Fig. 13a and c). The predicted volume and saturation changes against suction are somewhat less accurate, but still quite close to observations (Fig. 13b and d).

Sun et al. [26] also presented triaxial compression test data on compacted Pearl clay under constant mean net stress ($\bar{p} = 200$ kPa). Two of such tests were performed at a constant suction of 100 kPa (see Figs. 14 and 15), and the other two at a suction of 150 kPa (see Figs. 16 and 17). To investigate the influence of the degree of saturation on the stress–strain responses, Sun et al. [26] set the initial degrees of saturation (S_{ri}) to two different values for each suction level. All the test results are replotted in Figs. 14–17 and compared with the model predictions. Figures labelled with (a) in Figs. 14–17 show the stress–strain relationships in the planes of $\bar{\sigma}_1/\bar{\sigma}_3$ (the ratio between net axial stress and net confining stress) vs. ε_1 (axial strain) or ε_3 (lateral strain). Figures labelled with (b) show the suction variation during triaxial compression in the plane of s vs. ε_1. Figures labelled with (c) show the saturation variation during triaxial compression in the plane of S_r vs. ε_1. The initial states of the soil for each figure are listed in Table 4. The test results show that both the suction level and the saturation status affect the stress–strain relationships under triaxial conditions. The comparison between Figs. 14 and 15 and that between Figs. 16 and 17 indicate the degree of saturation can affect the stress–strain

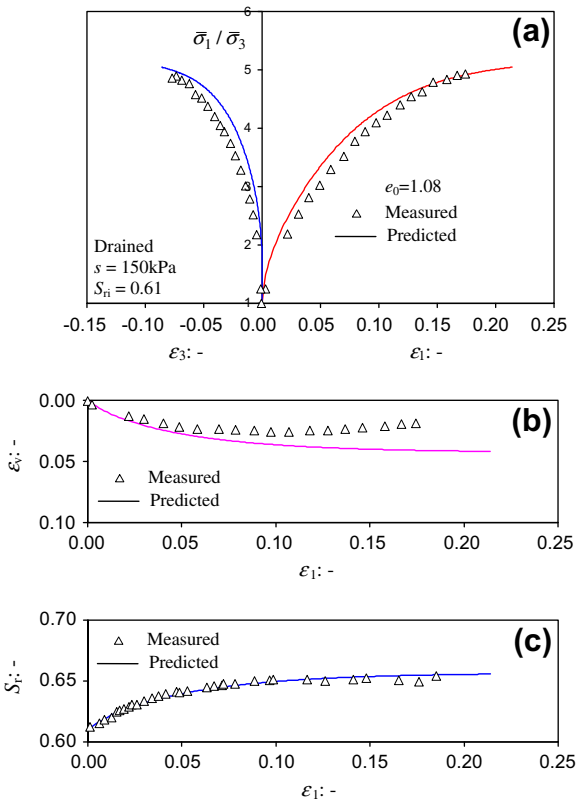

Fig. 16. Experimental results (data after [26]) of suction-controlled triaxial compression test on compacted Pearl clay ($s = 150$ kPa, $S_{ri} = 0.61$) as well as model simulations: (a) $\bar{\sigma}_1/\bar{\sigma}_3$ vs. ε_1 and ε_3, (b) ε_v vs. ε_1 and (c) S_r vs. ε_1.

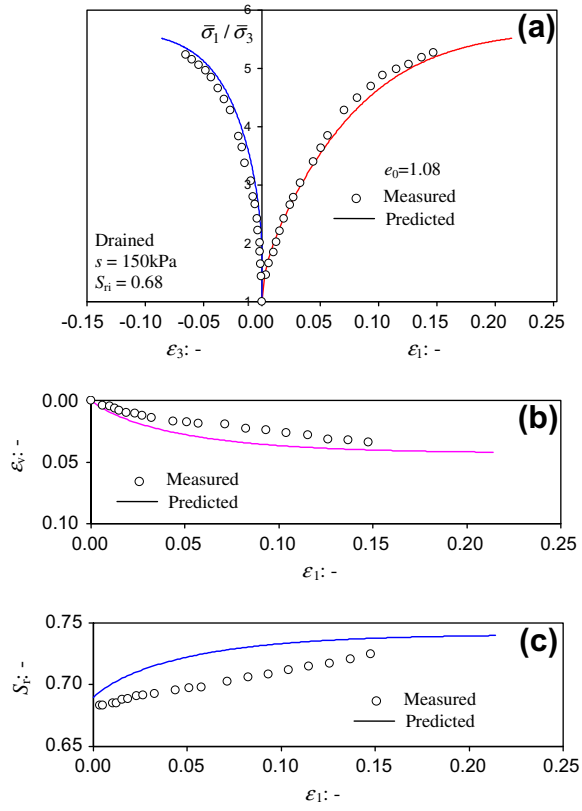

Fig. 17. Experimental results (data after [26]) of suction-controlled triaxial compression test on compacted Pearl clay ($s = 150$ kPa, $S_{ri} = 0.68$) as well as model simulations: (a) $\bar{\sigma}_1/\bar{\sigma}_3$ vs. ε_1 and ε_3, (b) ε_v vs. ε_1 and (c) S_r vs. ε_1.

Table 4
Initial states of different suction-controlled triaxial compression tests for compacted Pearl clay.

Figure No.	Suction (kPa)	Initial void ratio (–)	Mean net stress (kPa)	Initial degree of saturation (–)
Fig. 14	100	1.15	200	0.60
Fig. 15	100	1.12	200	0.77
Fig. 16	150	1.08	200	0.61
Fig. 17	150	1.08	200	0.68

relationships even if suction keeps constant. For example, with the same suction and initial density, the specimen with higher initial degree of saturation usually show higher critical state stress ratio. In addition, the negative dilatancy due to shearing leads to an increase in the degree of saturation and this also affects the stress–strain relationship. It can be seen that the proposed model predicts satisfactorily well the mechanical and hydraulic behaviour of the unsaturated compacted Pearl clay under triaxial conditions.

Finally, in addition to the suction-controlled triaxial tests, Sun et al. [25] presented results for an undrained triaxial test on unsaturated compacted Pearl clay. The initial suction is 65 kPa, the initial degree of saturation is 0.7, and the initial void ratio is 1.20. During the test, the confining net pressure ($\bar{\sigma}_3$) was kept constant at 100 kPa and the drainage valve was closed to maintain undrained conditions. The test data and model predictions are shown in Fig. 18. The proposed model again gives good predictions of the stress–strain behaviour as well as the suction changes and hydraulic response.

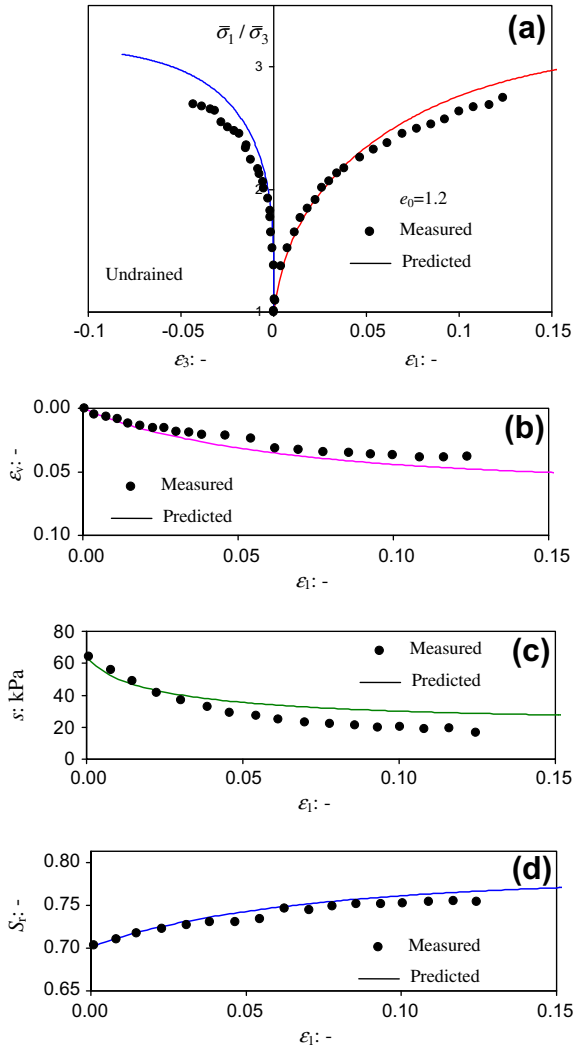

Fig. 18. Experimental results (data after [25]) of undrained triaxial compression test on compacted Pearl clay as well as model simulations: (a) $\bar{\sigma}_1/\bar{\sigma}_3$ vs. ε_1 and ε_3, (b) ε_v vs. ε_1, (c) s vs. ε_1 and (d) S_r vs. ε_1.

5. Concluding remarks

Constitutive relationships for general 3D stress states are derived from the new volume change equation proposed in the companion paper [37] and these relationships are formulated in the plane of the effective degree of saturation and the Bishop effective stress. The volume change equation is also used to derive the yield surface under triaxial stress state, following the same framework of the SFG model [17]. Similarly to the volume change equation, yield stress and shear strength are defined in terms of the Bishop effective stress and the effective degree of saturation, thus eliminating suction from the mechanical constitutive equations. Qualitative predictions of the model show that it can reproduce a number of key features of reconstituted London clay and compacted Pearl clay under isotropic/triaxial and drained/undrained conditions.

The major advantages of the proposed model include: (1) it can describe the non-linear compressibility of the soil under constant suction in a continuous and smooth manner; (2) it can explain many basic mechanical responses of unsaturated soils, such as drying induced shrinkage, wetting induced collapse and loading induced saturation; (3) it is a fully coupled model that can take into account the bi-directional hydro-mechanical interaction; (4) all the parameters used in the model have explicit physical meanings and can be calibrated via conventional laboratory tests. The main limitations of the proposed model include: (1) the proposed model is based the Modified Cam-clay model and is hence less applicable to shear-dilatant soils; (2) the adoption of a linear effective stress ($\sigma'_{ij} = \bar{\sigma}_{ij} + S_e s \delta_{ij}$) might lead to over-prediction of the critical strength at high suction values. A non-linear effective stress ($\sigma'_{ij} = \bar{\sigma}_{ij} + (S_e)^{a_3} s \delta_{ij}$) may lead to better predictions of the shear strength of unsaturated soils.

Compared with the existing constitutive models for unsaturated soils, the most distinguished feature of the proposed model is that the degree of saturation is used to replace suction as the complementary constitutive variable. The individual components of the model, such as the volume change, water retention, yield surface, shear strength and hydromechanical coupling, are defined in a mutually consistent manner. In this respect, the approach has similarities with the SFG model by Sheng et al. [17].

References

[1] Alonso EE, Gens A, Josa A. A constitutive model for partially saturated soils. Geotechnique 1990;40(3):405–30.
[2] Alonso EE, Pereira JM, Vaunat J, Olivella S. A microstructurally based effective stress for unsaturated soils. Geotechnique 2010;60(12):913–25.
[3] Bardet JP. A bounding surface model for sands. J Eng Mech, ASCE 1986;112:1198–217.
[4] Chiu CF, Ng CWW. A state-dependent elasto-plastic model for saturated and unsaturated soils. Geotechnique 2003;53(9):809–29.
[5] Cunningham MR, Ridley AM, Dineen K, Burland JB. The mechanical behaviour of a reconstituted unsaturated silty clay. Geotechnique 2003;53(2):183–94.
[6] Dafalias YF. Bounding surface plasticity. I: theory. J Eng Mech, ASCE 1986;112:1242–91.

[7] Gallipoli D, Wheeler SJ, Karstunen M. Modelling of variation of degree of saturation in a deformable unsaturated soil. Geotechnique 2003;53(1):105–12.
[8] Hashiguchi K. Subloading surface model in unconventional plasticity. Int J Soilds Struct 1989;25(8):917–45.
[9] Kohgo Y. An introduction of jumped kinematic hardening rule to elastoplastic model for unsaturated geo-materials. In: Alonso EE, Gens A, editors. Unsaturated soils, vol. 2. Barcelona (Spain): CRC Press; 2011. p. 857–62.
[10] Morvan M, Wong H, Branque D. An unsaturated soil model with minimal number of parameters based on bounding surface plasticity. Int J Numer Anal Meth Geomech 2010;34(14):1512–37.
[11] Ng CWW, Chiu ACF. Behaviour of loosely compacted unsaturated volcanic soil. J Geotech Geoenviron Eng, ASCE 2001;127(12):1027–36.
[12] Pereira JM, De Gennaro V. On the time-dependent behaviour of unsaturated geomaterials. In: Alonso EE, Gens A, editors. Unsaturated soils, vol. 2. Barcelona (Spain): CRC Press; 2011. p. 921–5.
[13] Roscoe KH, Burland JB. On the generalised stress–strain behavior of 'wet' clay. In: Heyman J, Leckie FA, editors. Engineering plasticity. Cambridge (England): Cambridge University Press; 1968. p. 535–609.
[14] Roscoe KH, Schofield AN, Thurairajah A. Yielding of clay in states wetter than critical. Geotechnique 1963;13:211–40.
[15] Schofield AN, Wroth CP. Critical state soil mechanics. London: McGraw-Hill; 1968.
[16] Sharma R. Mechanical behaviour of unsaturated highly expansive soil, PhD thesis, University of Oxford, UK; 1998.
[17] Sheng D, Fredlund DG, Gens A. A new modelling approach for unsaturated soils using independent stress variables. Can Geotech J 2008;45(4):511–34.
[18] Sheng D, Sloan SW, Yu HS. Aspects of finite element implementation of critical state models. Comput Mech 2000;26(2):185–96.
[19] Sheng D, Zhou AN, Fredlund DG. Shear strength criteria for unsaturated soils. Geotech Geol Eng 2011;29(2):145–59.
[20] Sun DA, Cui HB, Matsuoka H, Sheng D. A three-dimensional elastoplastic model for unsaturated compacted soils with hydraulic hysteresis. Soils Found 2007;47(2):253–64.
[21] Sun DA, Matsuoka H, Xu Y. Collapse behaviour of compacted clays by suction controlled triaxial tests. Geotech Test J, ASTM 2004;27(4):362–70.
[22] Sun DA, Matsuoka H, Yao YP, Ichihara W. An elastoplastic model for unsaturated soil in three-dimensional stresses. Soils Found 2000;40(3):17–28.
[23] Sun DA, Sheng D, Cui HB, Sloan SW. A density-dependent elastoplastic hydro-mechanical model for unsaturated compacted soils. Int J Numer Anal Meth Geomech 2007;31:1257–79.
[24] Sun DA, Sheng D, Sloan SW. Elastoplastic modelling of hydraulic and stress–strain behaviour of unsaturated soils. Mech Mater 2007;39(3): 212–21.
[25] Sun DA, Sheng D, Xiang L, Sloan SW. Elastoplastic prediction of hydro-mechanical behaviour of unsaturated soils under undrained conditions. Comput Geotech 2008;35(6):845–52.
[26] Sun DA, Sun WJ, Xiang L. Effect of degree of saturation on mechanical behaviour of unsaturated soils and its elastoplastic simulation. Comput Geotech 2009;37(5):678–88.
[27] Tarantino A. A water retention model for deformable soils. Geotechnique 2009;59(9):751–62.
[28] Toll DG. A framework for unsaturated soil behaviour. Geotechnique 1990;40(1):31–44.
[29] Toll DG, Ong BH. Critical state parameters for an unsaturated residual sandy clay. Geotechnique 2003;53(1):93–103.
[30] Tsiampousi A, Zdravkovic L, Potts DM. Modelling of overconsolidated unsaturated soils. In: Buzzi O, Fityus S, Sheng D, editors. Unsaturated soils – theoretical and numerical advances in unsaturated soil mechanics. Newcastle (Australia): CRC Press; 2010.
[31] van Genuchten MT. A closed-form equation for predicting the hydraulic conductivity of unsaturated soils. Soil Sci Soc Am J 1980;44:892–8.
[32] Yang C, Cui YJ, Pereira JM, Huang MS. A constitutive model for unsaturated cemented soils under cyclic loading. Comput Geotech 2008;35:853–9.
[33] Yao YP, Hou W, Zhou AN. UH model: three-dimensional unified hardening model for overconsolidated clays. Geotechnique 2009;59(5):451–69.
[34] Yao YP, Zhou AN, Lu DC. Extended transformed stress space for geomaterials and its application. J Eng Mech 2007;133(10):1115–23.
[35] Yin JH, Graham J. Elastic viscoplastic modelling of time-dependent stress–strain behaviour of soils. Can Geotech J 1999;36(4):736–45.
[36] Zhang F, Ikariya T. A new model for unsaturated soil using skeleton stress and degree of saturation as state variables. Soils Found 2011;51(1):67–81.
[37] Zhou AN, Sheng D, Scott SW, Gens A. Interpretation of unsaturated soil behaviour in the stress–saturation space, I: volume change and water retention behaviours. Comput Geotech, in preparation.